

# Space Weather®

## RESEARCH ARTICLE

10.1029/2022SW003292

### Key Points:

- Time-dependent solar irradiance data and highly physical effects are considered for solar radiation pressure (SRP) modeling
- With an enhanced SRP, the systematic correlation of solar radiation is largely reduced in low Earth orbit (LEO) precise orbit determination (POD)
- Enhanced dynamic models reduce the dependence on empirical parameters in LEO POD and improve the overall accuracy of satellite orbits

### Supporting Information:

Supporting Information may be found in the online version of this article.

### Correspondence to:

M. Li and K. Jiang,  
limin@whu.edu.cn;  
kc.jiang@whu.edu.cn

### Citation:

Wang, Y., Li, M., Jiang, K., Li, W., Zhao, Q., Fang, R., et al. (2023). Improving precise orbit determination of LEO satellites using enhanced solar radiation pressure modeling. *Space Weather*, 21, e2022SW003292. <https://doi.org/10.1029/2022SW003292>

Received 16 SEP 2022

Accepted 22 DEC 2022

### Author Contributions:

**Conceptualization:** Youcun Wang  
**Data curation:** Kecai Jiang  
**Formal analysis:** Youcun Wang, Na Wei, Renhai Mu  
**Funding acquisition:** Wenwen Li, Qile Zhao, Rongxin Fang, Na Wei  
**Investigation:** Youcun Wang  
**Methodology:** Youcun Wang, Wenwen Li  
**Project Administration:** Min Li, Qile Zhao  
**Software:** Min Li, Qile Zhao  
**Supervision:** Kecai Jiang, Wenwen Li  
**Validation:** Youcun Wang, Kecai Jiang

© 2023. The Authors.

This is an open access article under the terms of the [Creative Commons Attribution License](#), which permits use, distribution and reproduction in any medium, provided the original work is properly cited.

## Improving Precise Orbit Determination of LEO Satellites Using Enhanced Solar Radiation Pressure Modeling

Youcun Wang<sup>1</sup>, Min Li<sup>1</sup> , Kecai Jiang<sup>1</sup>, Wenwen Li<sup>1</sup> , Qile Zhao<sup>1</sup> , Rongxin Fang<sup>1</sup> , Na Wei<sup>1</sup> , and Renhai Mu<sup>1</sup>

<sup>1</sup>GNSS Research Center, Wuhan University, Wuhan, China

**Abstract** Precise orbit knowledge is a fundamental requirement for low Earth orbit (LEO) satellites. High-precision non-gravitational force modeling directly improves the overall quality of LEO precise orbit determination (POD). To address the potential systematic errors in solar radiation pressure (SRP), we introduce observed radiation data and modeled physical effects to describe the real in-flight environment of satellites. Time-dependent solar irradiance data and a highly physical shadow model are considered for SRP modeling. We develop an advanced thermal reradiation model for satellite solar panels. A set of improved non-gravitational force models is performed for LEO POD, and we discuss the benefits of the enhanced dynamic models on orbit quality and dependence on empirical parameters. The Gravity Recovery and Climate Experiment Follow-On (GRACE-FO), Jason-3, and Haiyang-2B missions are selected for the POD process. Estimated empirical acceleration and scale parameters and independent satellite laser ranging (SLR) are used to validate the final orbit solutions. The magnitude of empirical acceleration estimated in POD is reduced by 19% with the enhanced dynamic modeling, and the estimated scale factor for the SRP converges to stable and reasonable level. Furthermore, the steady-state temperature model used in thermal reradiation can effectively reduce mismodeled effects in the SRP, and the systematic linear dependency revealed by the SLR residuals is significantly reduced for the GRACE-C and Jason-3 satellites, with improvements of approximately 61% and 49%, respectively. Overall, advances are made in the explicit modeling of non-gravitational forces to pursue superior satellite orbits, suggesting a more dynamic orbit solution.

**Plain Language Summary** Decades of observations from the Gravity Recovery and Climate Experiment (GRACE) and GRACE Follow-On and altimetry missions, such as the TOPEX/Poseidon and Jason-1/2/3 satellites, have greatly helped us understand the Earth, and these low Earth orbit (LEO) missions depend crucially on accurate orbit information. The interaction of photons with a satellite surface is very important, as one of the non-gravitational forces acting on a satellite and consistently affecting satellite orbit accuracy. In this study, modeled highly physical effects are considered for the enhanced solar radiation pressure (SRP) to obtain superior POD performance. Measured radiation data are used to account for SRP acceleration instead of the previous solar constant, and a realistic shadowing process is introduced to describe the geometric relationship of the satellite with the Sun and the Earth. Moreover, an advanced thermal reradiation model is proposed to compute the SRP accelerations of the satellite body and solar panels. The results show that the enhanced orbit solution reduces the dependence on empirical parameters and is beneficial for the overall quality of satellite orbits. This is in line with our goal of finding the optimal solution to obtain the best-possible orbits.

## 1. Introduction

Low Earth orbit (LEO) satellites play an important role in the field of Earth observation, and decades of observations have greatly helped us understand the Earth. Among them, gravity detection and satellite altimetry missions require accurate orbits to support their operation. Reduced-dynamic precise orbit determination (POD) developed by Wu et al. (1991) currently represents a well-established technique and is widely applied for LEO missions requiring the utmost orbit precision and accuracy (Fernández et al., 2022; Hackel et al., 2016; Li et al., 2017; Montenbruck, Kunzi, & Hauschild, 2021). Based on an accurate conservative force model, this method makes use of scale parameters for non-gravitational forces and empirical accelerations to address the uncertainty in orbit determination.

Accurate modeling of non-gravitational force is required for the precise orbit determination of LEO satellites (Hackel et al., 2016; Kang et al., 2006; Montenbruck, Hackel, & Jäggi, 2018; Wu et al., 1991), SLR satellites

**Visualization:** Youcun Wang, Rongxin Fang, Renhai Mu

**Writing – original draft:** Youcun Wang, Min Li

**Writing – review & editing:** Youcun Wang, Min Li, Rongxin Fang

(Appleby et al., 2016; M Pearlman, Arnold, et al., 2019; Zajdel et al., 2022), and GNSS satellites (D. Arnold et al., 2015; Bury et al., 2020; Duan et al., 2020; Montenbruck et al., 2014; Zhao et al., 2022). Solar radiation pressure and atmospheric drag are the two most important non-gravitational forces acting on LEO satellites. Atmospheric drag describes the interaction force of atmospheric gases with the satellite surface, which is mainly related to the atmospheric density and satellite structural property. The SRP, on the other hand, describes the absorption and reflection of solar radiation at the satellite surface. The calculation of drag and SRP acceleration acting on a satellite is based on the establishment of a macro-model of the satellite.

The TOPEX/Poseidon altimetry satellite (W. I. Bertiger et al., 1994) was the first to use a box-wing macro-model to describe the satellite shape, which divided the satellite structure into two parts: the body and the solar array (Marshall & Luthcke, 1994). Subsequent altimetry missions, such as Jason-1/2/3 (Cerri et al., 2010; Haines et al., 2004) and Sentinel-3A/B (Montenbruck, Hackel, & Jäggi, 2018), have employed the same model to describe the satellite geometry. For LEO missions such as the Gravity Recovery and Climate Experiment (GRACE), GRACE Follow-On (GRACE-FO) (Tapley et al., 2004; Kornfeld et al., 2019), and the Swarm mission (Friis-Christensen et al., 2008), where the solar cells are mounted on the satellite body, a panel-dependent macro model is considered. Accurate modeling of satellite geometry is gradually carried out on LEO satellites. Finite element modeling is employed for GRACE accelerometer calibration (Woske et al., 2019), and high-fidelity geometry modeling for CHAMP, GRACE, GOCE, and Swarm is used for thermospheric density determination (March et al., 2019).

The standard analytical SRP model developed by (Marshall & Luthcke, 1994; Milani et al., 1987) was first implemented for POD of the TOPEX/Poseidon satellite and was widely adopted in subsequent LEO missions (Jaggi et al., 2016; Li et al., 2017; Montenbruck, Hackel, & Jäggi, 2018; van den Ijssel et al., 2015). However, the analytical SRP model only considers the visible radiation of the Sun (Montenbruck et al., 2014), and in fact, this modeling is imperfect. The radiation pressure coefficient of a LEO satellite surface depends on the wavelength of incoming photons (Fröhlich & Lean, 2004; Prölss & Bird, 2004). The introduction of dual channels of the solar spectrum has significantly improved the accelerometer calibration of GRACE (Vielberg & Kusche, 2020). The visible and infrared radiation coefficients of the SRP are considered in high-quality LEO POD (Mao et al., 2021; Montenbruck, Hackel, van den Ijssel, & Arnold, 2018; Montenbruck, Hackel, et al., 2021). Additionally, the magnitude of the SRP depends on the solar flux near the Earth's surface, and a solar constant of 1367 w/m<sup>2</sup> is usually used to account for the solar flux at one astronomical unit (AU) (Montenbruck et al., 2014). The actual solar irradiance varies with the solar cycle and solar activity (Fröhlich & Lean, 2004). A shadow function is used to describe the geometric relationship between the Sun, the Earth, and satellites. The conical shadow model from Montenbruck et al. (2002) is widely used to describe the penumbra transition of LEO satellites. A spherical Earth is considered in the umbra and penumbra regions, whereas in reality, it ignores the Earth's oblateness and the effects of atmospheric refraction, which will inevitably affect the calculation of the SRP acceleration during penumbra. The case of a lunar eclipse is not considered in this paper, and radiation from stellar sources other than the Earth and Sun is not considered. The thermal reradiation caused by the SRP absorption is usually treated with a simple static model or ignored (Montenbruck et al., 2014; Woske et al., 2019). The calibrated GRACE accelerometer measurements deteriorate when the instantaneous thermal reradiation pressure (TRP) is used (Vielberg & Kusche, 2020). Woske et al. (2019) found that there was a clear periodic error in the accelerometer calibration of GRACE-A for the static TRP model.

Similar to SRP modeling, the Earth radiation pressure (ERP) depends on the radiation of the Earth, satellite materials, and surface area. In comparison with the SRP, the amount of radiation reflected or emitted from the Earth's surface is essential for the accurate calculation of the ERP. A ring-like discretization of the source of radiation, resulting in dozens of surface elements, is implemented in Knocke et al. (1988) and Rodriguez-Solano et al. (2011). For a more realistic model, high-resolution Earth radiation data supported by the Clouds and the Earth's Radiant Energy System (CERES) Science Team are applied (Mao et al., 2021; Montenbruck, Hackel, & Jäggi, 2018; Vielberg & Kusche, 2020; Visser et al., 2019). For POD, we employed hourly CERES SYN1deg Earth observation data (CERES, Science Team 2017) to represent the Earth's emissivity and reflectivity.

In this work, we present enhanced non-gravitational force modeling to implement POD for LEO satellites and demonstrate a notable improvement in the overall orbit quality. The preliminary motivation of this study was to solve simplifications or potential systematic errors in non-gravitational force modeling. These models can aid in improving POD, gravity field recovery, and satellite altimetry. For SRP modeling, we consider the radiation

pressure from two channels of the solar spectrum, and time-dependent radiation data are used to replace the solar constant. Subsequently, a highly physical shadow model (R. Robertson et al., 2015) is considered during the penumbra transitions of LEO satellites. Simple static and steady-state temperature models are extended for the TRP calculations of satellite surfaces. When modeling atmospheric drag, we do not treat atmospheric density modeling but employ the latest DTM-2020 (Drag Temperature Model) model for drag calculation.

This paper is organized as follows. The detailed SRP modeling method for LEO satellites is presented in Section 2. Then, the data process strategies and orbit models used for POD are summarized in Section 3. In Section 4, we analyze and discuss the POD performance of different orbit solutions. Finally, we summarize this article and give a general outlook in Section 5.

## 2. Enhanced Solar Radiation Pressure Modeling

For LEO reduced-dynamic POD, the main gravitational forces can be numerically computed using existing state-of-the-art models. The modeling of non-gravitational forces is a challenging task, as it often relies on various auxiliary products (such as the solar flux and geomagnetic activity data for drag and Earth radiation data for the ERP), while on the other hand, the real in-flight perturbation environment is hard to describe. In our research, explicit modeling of non-gravitational forces can be advanced using an enhanced solar radiation pressure. Modeled physical effects are considered for refined SRP modeling, which is the goal of this study. The common conical model is replaced by a physical shadow model that considers atmospheric effects and assumes an oblate Earth. The assumptions and conditions for two different thermal radiation models at the satellite surface are described. In addition, time-dependent radiation data products are used, which may lead to the reduction of systematic errors in the SRP. Specific aspects of SRP modeling are discussed in this section.

### 2.1. Analytical SRP Model

The origin and effects of the SRP are the interactions between photons and satellite surface materials illuminated by the Sun (Milani et al., 1987; Montenbruck et al., 2002). For a single flat surface, the acceleration caused by the SRP can be described as

$$a_{\text{SRP}} = -\frac{\Phi}{c} \frac{A}{m} C_R \cos(\theta) \frac{1}{2} (C_{R_{\text{SW}}}^{\odot} + C_{R_{\text{LW}}}^{\odot}) v. \quad (1)$$

This analytical SRP model combines the radiation pressure equation in Milani et al. (1987) with the wavelength-dependent radiation pressure coefficient (Vielberg & Kusche, 2020), where  $\Phi$  denotes the solar radiation pressure,  $c$  is the speed of light,  $A$  is the area of the satellite surface panel and  $m$  is the total mass of the spacecraft. The scaling parameter  $C_R$  is estimated in POD to absorb the remaining deficiencies of modeled forces and spacecraft parameters.  $\theta$  denotes the angle between the satellite surface normal and the incident radiation. The radiation coefficients result from two channels of the solar spectrum (visible  $C_{R_{\text{SW}}}^{\odot}$  and infrared  $C_{R_{\text{LW}}}^{\odot}$ ) instead of visible wavelengths only. Furthermore, the SRP depends on the Sun-satellite-Earth geometry (shadow function  $v$ ), which indicates whether the satellite is in umbra, penumbra, or sunlight. The thermo-optical properties of satellite surfaces are essential for SRP models. Commonly, the material properties of LEO missions are available for visible and infrared radiation within the macro-model. The wavelength-dependent radiation pressure coefficient  $C_R^{\odot}(\lambda)$  models the interaction of incoming photons with an individual plate (Doornbos, 2012; Marshall & Luthcke, 1994). Specular ( $c_d$ ) and diffuse ( $c_s$ ) reflections and absorption ( $c_a$ ) of photons are considered as

$$C_R^{\odot}(\lambda) = c_d \left( s - \frac{2}{3} n \right) - c_s 2 \cos \theta n + c_a s. \quad (2)$$

Here,  $s$  is the unit vector of the satellite to the Sun, and  $n$  is the satellite surface normal. In Equation 1, two channels for the solar spectrum are used and weighed with 1/2, assuming that 50% of the total SRP acceleration is caused by both longwave and shortwave radiation (Vielberg & Kusche, 2020).

### 2.2. Variability of Solar Irradiance

The magnitude of SRP acceleration depends on solar irradiance. The radiation pressure of the Sun in the vicinity of the Earth can be obtained as

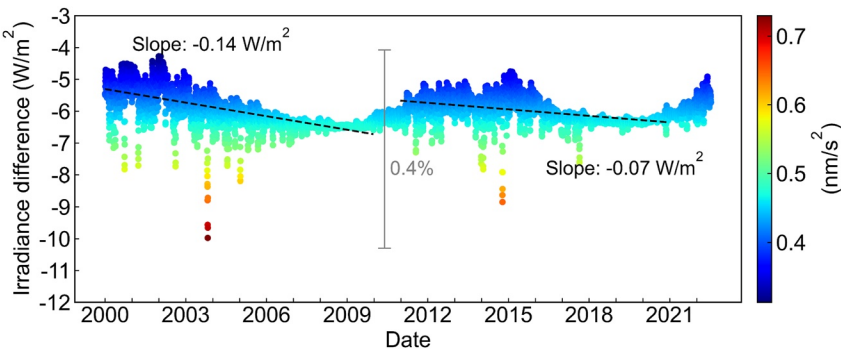


**Figure 1.** Irradiance difference between the solar constant and the total solar irradiance measurements. The SRP acceleration difference due to the time-dependent TSI product is shown by the color scale bar on the right.

$$\Phi = \left( \frac{1\text{AU}}{r_\odot} \right)^2 P_{\odot,\text{IAU}} \quad (3)$$

where  $r_\odot$  is the instantaneous distance from the Sun to the satellite and the Sun position can be computed from JPL planetary ephemerides (Park et al., 2021). Here, an astronomical unit (1AU) denotes the mean Sun-Earth distance. The solar radiation pressure ( $P_{\odot,\text{IAU}}$ ) at 1 AU is commonly approximated as 1367 W/m<sup>2</sup> (Montenbruck et al., 2014), whereas in reality, the total solar irradiance (TSI) varies with the solar rotation and the solar cycle (Dewitte & Nevens, 2016; Kopp & Lean, 2011). A total solar irradiance of 1360.5 W/m<sup>2</sup> during the 2008 solar minimum period can be obtained (Kopp & Lean, 2011).

In this paper, the daily TSI product is considered to account for the solar radiation pressure at 1 AU instead of the solar constant. Measured TSI data can be accessed from [https://ceres.larc.nasa.gov/documents/TSIdata/CERES\\_EBAF\\_Ed2.8\\_DailyTSI.txt](https://ceres.larc.nasa.gov/documents/TSIdata/CERES_EBAF_Ed2.8_DailyTSI.txt). Details of these data and implementation are described in Nasa/Larc/Sd/Asdc (2019). The TSI time series data, which varied between 1357 and 1363 W/m<sup>2</sup> after 2000, is shown in Figure 1. For the Jason-3 satellite with solar panels, direct SRP accelerations caused by a solar irradiance of 1367 W/m<sup>2</sup> can reach a magnitude of 100 nm/s<sup>2</sup>, and the resulting SRP acceleration of the LEO satellite due to irradiance difference is within 1 nm/s<sup>2</sup> (Figure 1). The solar flux largely depends on the solar cycle and the solar rotation with periods of approximately 11 years and 27 days, respectively. The annual rate of change according to the solar cycle is shown in Figure 1. Then, the time-dependent incident solar flux is given by

$$\Phi_{TSI} = \left( \frac{1\text{AU}}{r_\odot} \right)^2 P_{\odot,\text{IAU}}(t). \quad (4)$$

### 2.3. Physical Shadow Model

The shadow function  $v$  is taken into account for the Sun illumination of a satellite. The conical shadow model is widely used to identify eclipse transitions, which can distinguish between umbra, penumbra, or sunlight (Montenbruck et al., 2002). The conical shadow model assumes a spherical Earth, and the absorption, scattering, and refraction of light in the atmosphere are not considered. In this study, a more advanced physical model developed by R. V Robertson (2015) is applied for POD. The curve-fitted Solar radiation pressure with Oblateness and Lower Atmospheric Absorption, Refraction, and Scattering (SOLAARS) model (R. V. Robertson, 2015) is based on the assumption of an oblate Earth and consideration of atmospheric effects. The evolution of the conical shadow model (Montenbruck et al., 2002) and physical model (R. V. Robertson, 2015) during a typical penumbra transition is displayed in Figure 2. Compared with the conical shadow, the SRP acceleration difference in the penumbra period can reach 5 nm/s<sup>2</sup> in the local orbital system.

### 2.4. Thermal Reradiation for Satellite Body and Solar Panels

The effects of solar radiation are twofold. The direct radiation from the Sun is the origin of the SRP force. The secondary effect is the thermal reradiation pressure (TRP) of the satellite itself due to the absorbed radiation,

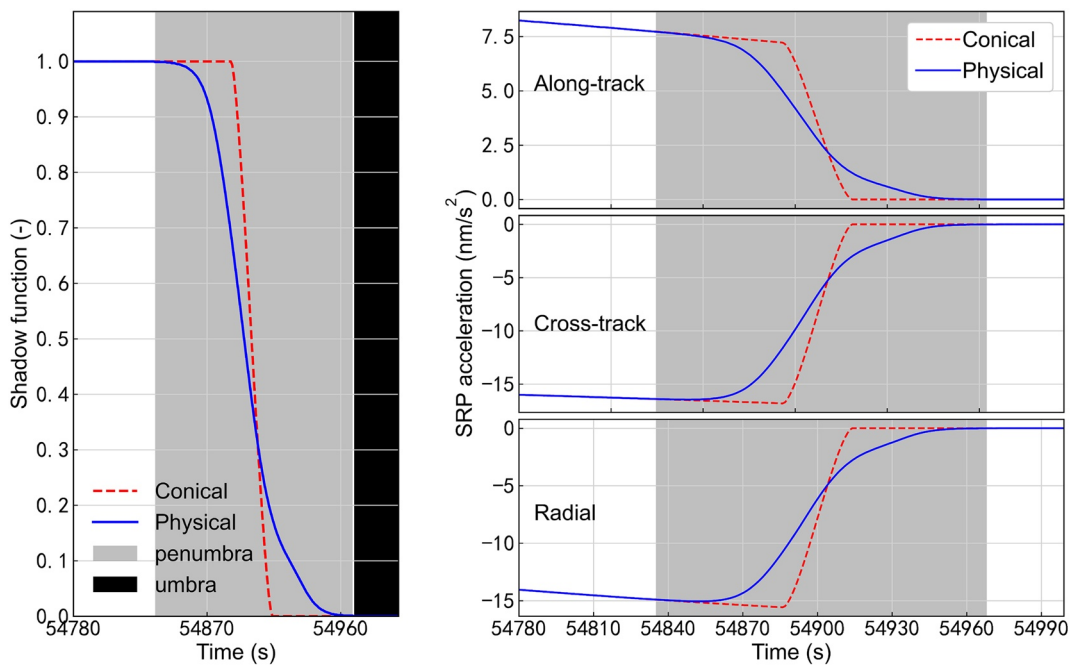


**Figure 2.** Typical shadow crossing of the GRACE-FO satellite on 1 January 2019. SRP accelerations resulting from the conical model (red) and SOLAARS-CF (blue) are shown. The shaded area represents the penumbra period.

which is in accord with the Stefan–Boltzmann law. The thermo-optical properties of the satellite surface are essential for the computation of the TRP. In some cases, the TRP may account for up to 25% of the SRP (Woske et al., 2019). In this study, we considered two different models to compute the TPR of LEO satellites: (a) a static temperature model and (b) a steady-state temperature model. The basic assumptions for the two different models are depicted in Figure 3.

The most common way to account for TRP accelerations is to assume instantaneous reradiation of heat for the satellite surface (Montenbruck et al., 2014; Vielberg & Kusche, 2020). For a simple static temperature model, the thermal reradiation resulting from the satellite body and solar panel is performed in different ways (Figure 3). The thermal reradiation  $q_{\text{rad}}$  of the satellite body is equal to the absorbed incoming radiation  $q_{\text{rad}}^{\text{in}}$  (Montenbruck et al., 2014), and the TRP accelerations of the satellite body are given by

$$\begin{aligned} q_{\text{rad}}^{\text{in}} &= q_{\text{rad}} \\ a_{\text{TRP, body}} &= -\frac{2}{3} \frac{\Phi}{c} \frac{A}{m} \cos(\theta) c_a \mathbf{n} \mathbf{v}. \end{aligned} \quad (5)$$

Considering the amount of power  $q_{\text{elec}}$  drawn from the solar panels to supply energy to satellite components, the thermal reradiation  $q_{\text{rad}}$  of the solar panels becomes

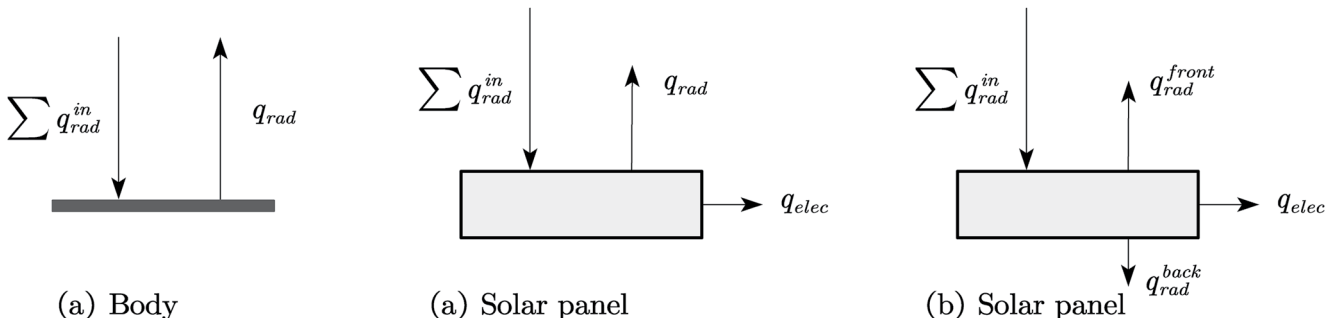


**Figure 3.** Assumptions and conditions for the static temperature model (a) and steady-state temperature model (b).

$$\begin{aligned} q_{\text{rad}}^{\text{in}} &= q_{\text{rad}} + q_{\text{elec}} \\ a_{\text{TRP,solar panel}} &= -\frac{2}{3} \frac{\Phi}{c} \frac{A}{m} (1 - C_{\text{cell}}) \cos(\theta) c_a \mathbf{n} \end{aligned} \quad (6)$$

where  $C_{\text{cell}}$  is the efficiency of the solar cells, and the material-related information can be obtained from space-craft manufacturers.

An advanced model considers heat transfer through the solar panel, and an energy balance is considered to compute the surface temperatures (Figure 3). The governing equation for the steady-state temperature of the solar panels is

$$\begin{aligned} q_{\text{in}} &= q_{\text{rad(front)}} + q_{\text{rad(rear)}} + q_{\text{elec}} \\ a_{\text{TRP,solar panel}} &= -\frac{2}{3} \frac{A}{m} \frac{\sigma}{c} (\varepsilon_{\text{front}} T_{\text{front}}^4 - \varepsilon_{\text{rear}} T_{\text{rear}}^4) \mathbf{n} \end{aligned} \quad (7)$$

where  $q_{\text{rad(front)}}$  and  $q_{\text{rad(rear)}}$  refer to the thermal reradiation of the front and back surfaces of the solar panels.  $\sigma$  is the Stefan-Boltzmann constant ( $5.67 \times 10^{-8} \text{ W m}^{-2} \text{ K}^{-4}$ ), and  $\varepsilon_{\text{front}}$  and  $\varepsilon_{\text{rear}}$  are the emissivity of the front and back surfaces, respectively. The temperatures of the front and back surfaces ( $T_{\text{front}}$  and  $T_{\text{rear}}$ ) can be solved numerically (Adhya, 2005). Considering that the spacecraft body is covered with multilayer insulation (MLI), the heat conduction of the body is not considered. Instantaneous thermal reradiation described by Equation 5 is employed to account for the TRP accelerations of the satellite body.

Subsequently, we plotted the SRP accelerations obtained from static temperature and steady-state temperature models for the GRACE-C satellite during January 2019 (Figure 4). Differences in modeled accelerations are obvious in the cross-track and radial directions and reach the maximum values around the orbit angle  $90^\circ - 180^\circ$ . Thus, this difference is clearly related to the direct solar irradiation of the satellite.

### 3. POD Models and Data Set

This section presents an overview of the orbit models and a set of improved strategies for LEO POD. Four typical LEO missions (the two GRACE-FO satellites, HY-2B, and Jason-3 satellites) are selected to validate the new POD strategies. As mentioned in Section 2, the enhanced SRP model is applied for LEO reduced-dynamic POD, and the satellite-specific data are described in the following.

#### 3.1. Data Set of LEO Missions

Precise orbit determination for the four LEO satellites is performed to investigate the performance of new non-gravitational forces modeling. A common period, the whole year of 2019, is selected for LEO POD in this study. The purpose of LEO missions and the POD package are briefly described below.

The Gravity Recovery and Climate Experiment Follow-On (GRACE-FO) mission is the second U.S.-German satellite mission for gravity measurement, and is the successor to the original GRACE mission (Landerer et al., 2020). New GRACE-FO satellites (namely, GRACE-C and GRACE-D) adopt the same formation-flying design of GRACE. New onboard equipment called a laser ranging interferometer (LRI) is employed for technology demonstration (Abich et al., 2019). A GPS receiver manufactured by JPL is used to support precise orbit determination (W. Bertiger et al., 2010; Kang et al., 2020), and a laser retro-reflector (LRR) manufactured by GFZ is employed to evaluate and enhance the orbit and gravity field solutions.

Jason-3 is the fourth U.S.-European altimetry mission, and it continues the study of ocean surface topography measurements, which was started by its predecessors (i.e., Jason-1/2 and Topex/Poseidon) (Haines et al., 2004; Lambin et al., 2010). Three different POD instruments, including a GPS receiver, a Doppler Orbitography and Radiopositioning Integrated by Satellite (DORIS) receiver, and an LRR array, are used to obtain the precise orbit of the satellite. Both the GPS and DORIS techniques enable continued observation coverage, providing two fully independent types of POD solutions (Flohrer et al., 2011; Montenbruck, Hackel, & Jäggi, 2018). HY-2B is the first routine satellite of the marine dynamic environment program planned by China (NSOAS, 2021). It focuses on the variations in ocean-surface height and ocean environment monitoring, similar to its predecessor (HY-2A)

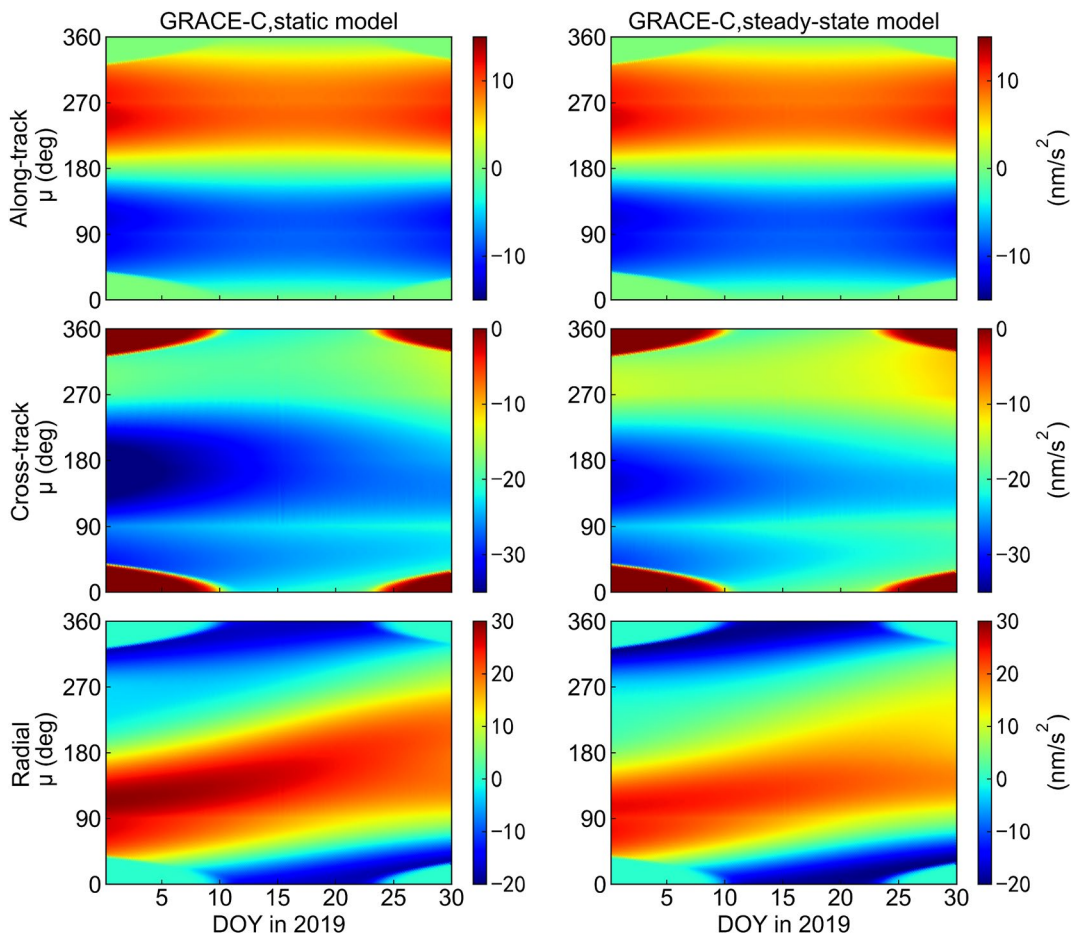


**Figure 4.** Modeled SRP accelerations acting on the GRACE-C satellite from the static model (left) and steady-state model (right) in the along-track, cross-track, and radial directions during January 2019.  $\mu$  denotes the orbit angle relative to the midnight point. Note the scale differences for each direction.

(Lin & Jia, 2022; J. Wang, Aouf, et al., 2020). A GPS receiver developed by the China Academy of Space Technology (CAST) is used to generate precise orbit solutions, and an official target accuracy of 2–3 cm in radial directions is specified (NSOAS, 2021).

### 3.2. POD Models

Reduced-dynamic POD relies on high-precision carrier phase observations and a dynamic orbit model. This approach makes use of scaling parameters for individual non-gravitational surface forces as well as empirical accelerations to compensate for unmodeled deficiencies (Wu et al., 1991). In addition, the initial position and velocity as well as receiver clock offsets and carrier phase ambiguities are adjusted based on the batch least squares estimator. The modified version of Positioning And Navigation Data Analyst (PANDA) (Liu & Ge, 2003) software is employed to generate precise orbit solutions. An overview of the employed models and POD strategy is summarized in Table 1.

The most important gravitational forces acting on LEO satellites are well described by the established models. Details of these models and references can be found in Table 1. However, it is less true for non-gravitational models such as radiation pressure and atmospheric drag. LEO missions usually carry various scientific instruments, and a plate-related macro-model is employed to approximate actual spacecraft geometry within this work. The total accelerations due to non-gravitational forces are computed based on the macro-model. The thermo-optical properties of the satellite surface (i.e., absorption and specular and diffuse reflection) are described in the visible and infrared regions to compute the SRP accelerations. Macro-models for all satellites taking into account the

**Table 1**  
*Overview of the Models and Data Sets for LEO POD*

|                            | Description   |
|----------------------------|---|
| Dynamic model              |   |
| Earth gravity              | EIGEN6C ( $120 \times 120$ ) (Shako et al., 2014)   |
| Solid Earth and pole tides | IERS 2010 conventions (Petit & Luzum, 2010)   |
| Ocean tides                | FES 2004 ( $30 \times 30$ ) (Lyard et al., 2006)  |
| N-body disturbance         | JPL DE405 (Standish & Williams, 1992)   |
| Relativity                 | Post-Newtonian correction   |
| Solar radiation pressure   | Plate-wise macro-model; radiation pressure coefficients (VIS and IR)<br>(Montenbruck et al., 2014); conical Earth shadow (Montenbruck et al., 2002);<br>Solar constant (Montenbruck et al., 2014)   |
| Earth radiation pressure   | Plate-wise macro-model, radiation pressure coefficients (VIS and IR); Outgoing<br>flux from SYN1deg data (CERES, 2017)  |
| Atmospheric drag           | Plate-wise macro-model; DTM-2020 atmospheric density model (Bruinsma &<br>Boniface, 2021); solar flux and geomagnetic activity data ( <a href="http://celestak.com/SpaceData/SW-All.txt">http://celestak.com/SpaceData/SW-All.txt</a> )           |
| Empirical acceleration     | One-cycle-per-revolution accelerations in along-track and cross-track directions  |
| Observation model          |   |
| Observation                | Undifferenced ionosphere-free code and carrier phase combinations   |
| Interval and arc length    | 30 s and 30 hr  |
| GPS orbit and clocks       | CNES-CLS “GRG” products; 30 s sampling (Loyer et al., 2012)   |
| GPS satellite biases       | CNES-CLS wide-lane satellite biases (Loyer et al., 2012)  |
| GPS satellite antenna      | IGS ATX models (Schmid et al., 2016)  |
| LEO GPS antenna            | PCO from ground calibration and PCV correction from in-flight calibration   |
| LEO attitude               | Quaternions from onboard star trackers  |
| Estimation                 |   |
| Estimator                  | Batch least squares   |
| Estimated parameters       | Position and velocity at the initial epoch; scale factors for SRP and drag; amplitudes<br>of circle-per-revolution acceleration of sine + cosine acting on along-track and<br>cross-track directions; epoch-wise clock offsets, phase ambiguities |
| SLR validation             |   |
| Station coordinates        | SLRF2014 (ILRS, 2020)   |
| Solid Earth and pole tides | IERS 2010 conventions (Petit & Luzum, 2010)   |
| Ocean tide loading         | FES 2004 (Lyard et al., 2006)   |
| Tropospheric delay         | Mendes and Pavlis (2004)  |
| Relativity                 | Space-time curvature correction   |

principal body shape and solar cells are provided by the respective manufacturers (see Tables S1–S4 in Supporting Information S1). The required daily solar flux and geomagnetic activity data are major input parameters to the atmospheric density model (See Table 1). The scale factors for the SRP and drag are estimated in POD to address prevailing uncertainties in spacecraft parameters and the in-flight environment. Piecewise empirical accelerations in the along-track and cross-track directions are adjusted as part of POD, which can be used as a quality indicator of employed force models. Considering that the radial acceleration of the ERP is the largest, the scale factor  $C_E$  is not estimated ( $C_E = 1$ ) to avoid the impact of potential radial orbit shifts. The erroneous phase center offset (PCO) or motion of the center-of-mass (CoM) may result in a similar effect at the same time (Montenbruck, Hackel, & Jäggi, 2018).

In comparison to the SRP, the acceleration caused by the ERP becomes less relevant. The ERP acceleration acting on a LEO satellite accounts for less than 10% of the SRP acceleration over the same period (Hackel et al., 2016;

Woske et al., 2019). Therefore, the detailed effects of the ERP are not considered in this study. The atmospheric forces due to the interaction of air molecules with the spacecraft surface are heavily dependent on the altitude of the satellite. For LEO satellites with very low altitudes, atmospheric drag is the most dominant nongravitational force (Doornbos, 2012; Montenbruck et al., 2002; Pérez & Bevilacqua, 2015). Atmospheric density is a critical input parameter for the accurate modeling of atmospheric drag. Some advanced atmosphere models (e.g., NRLMSISE-00, JB2008, and DTM2013) have been developed and tested in different publications (Bruinsma & Boniface, 2021; Doornbos, 2012; Vallado & Finkleman, 2014). Within this paper, the latest DTM model version (i.e., DTM-2020) developed by the Space Weather Atmosphere Models and Indices (SWAMI) project is employed.

Piecewise empirical acceleration has been widely used in LEO POD to compensate for the deficiencies in prior force models (Bock et al., 2014; Fernández et al., 2022; Y. C. Wang et al., 2021). The empirical accelerations are estimated in the along-track, cross-track, and radial directions, and they can be introduced as measure indicators for mismodeled effects, which are described in Montenbruck, Hackel, et al. (2021). A benefit of the accurate modeling of non-gravitational forces is to reduce the amount of empirical acceleration used for POD. Additionally, an erroneous antenna offset or CoM motion can be revealed by the bias in empirical accelerations. A systematic bias has been confirmed in the Sentinel-3A (Montenbruck, Hackel, & Jäggi, 2018) and Sentinel-6A (Montenbruck, Hackel, et al., 2021) satellites.

Details of the measurement-related parameters and employed data are given in Table 1. A consecutive 30-hr POD solution with a 6-hr overlap (between subsequent orbits) is applied in this work. The undifferenced ionosphere-free code and carrier phase combinations with 30 samplings are used for reduced-dynamic orbit determination, which is consistent with IGS high-rate GNSS clock products (Dow et al., 2009). The GPS orbit and clocks as well as satellite-specific biases provided by Center National d'Études Spatiales/Collecte Localisation Satellites (CNES/CLS) (Loyer et al., 2012) were used for single-receiver ambiguity resolution. Different from CNES/CLS products, the observable-specific signal biases (OSB) product obtained from the Center for Orbit Determination in Europe (CODE) (Schaer et al., 2021) or Wuhan University (WHU) (Geng et al., 2019) together with corresponding clock and orbit products are available to support single-receiver ambiguity fixing. Both strategies are equivalent, as described in Banville et al. (2020) and Zhang et al. (2021). For the LEO GPS receiver, the reference values of the nominal phase center offset (PCO) are provided by the respective manufacturer, and in-flight phase center variation (PCV) calibration is conducted using the residuals stacking approach (Jäggi et al., 2009). A new PCV map derived from enhanced dynamic orbit solutions is presented in Figure S1 in Supporting Information S1, and PCV differences due to phase residuals from different POD strategies are shown in Figure S1 in Supporting Information S1. The measured attitude data are employed to describe the instantaneous orientation of the spacecraft.

### 3.3. POD Processing Strategies

As discussed in Section 3.2, elaborate non-gravitational force modeling is developed to better describe the real in-flight environment for LEO satellites. Various external products and physical effects are considered to improve SRP modeling. Time-dependent Sun radiation data are employed to replace the solar constant. Earth oblateness corrections and atmospheric effects have been considered for an advanced physical shadow model. In addition to the simple static temperature model, a more realistic steady-state model is used to account for thermal reradiation pressure acting on the satellite body and solar panels. An improved atmospheric density model (i.e., DTM-2020) is employed to compute the atmospheric drag force in orbit determination.

Several processing strategies are considered for LEO POD using a modified version of PANDA software. For clear identification of orbit solutions, three three-digit identifiers (IDs) are used to distinguish different POD strategies, and implementation details are shown in Table 2. The SRP and drag models described in Table 1 are prudently defined as standard models (NG0) in this study. The atmospheric density based on DTM-2020 is employed in the orbit solution NG1, and NG2 considers TSI data and the physical shadow model. A static temperature model is introduced to account for the TRP of satellites in NG3, and an advanced steady-state temperature is considered in NG4. As shown in Table 2, the NG series represent different non-gravitational force modeling strategies, and the POD performance of these models is assessed.

**Table 2**  
Summary of POD Solutions Obtained From Different Strategies

| Solutions ID | DTM-2020 | SRP parameters             | Thermal reradiation |
|--------------|----------|----------------------------|---------------------|
| NG0          | No       | Conical and Solar constant | No                  |
| NG1          | Yes      | Conical and Solar constant | No                  |
| NG2          | Yes      | Physical and TSI           | No                  |
| NG3          | Yes      | Physical and TSI           | Static model        |
| NG4          | Yes      | Physical and TSI           | Steady-state model  |

## 4. Impact of the Enhanced SRP Model on LEO Satellite Orbits

In this section, we assess the impact of enhanced non-gravitational force modeling on POD performance. One-year observations of the GRACE-FO, HY-2B, and Jason-3 missions were selected to evaluate the precision of the orbit solutions, and the internal consistency indicators and external orbit validation were applied for orbit analysis. Empirical acceleration and scale parameters are counted for the assessment of potential unmodeled deficits. SLR observations are employed as a fully independent means to validate GNSS-based POD solutions.

### 4.1. Empirical Orbit Parameter Performance

For a reduced-dynamic approach, piecewise empirical accelerations and a global scale factor for SRP are estimated in POD iterations. The number of these parameters can be used to measure the dependence of the a priori model on empirical parameters (Hackel et al., 2016; Montenbruck, Hackel, et al., 2021). For the SRP model, a scale factor  $>1$  indicates an underestimated value, for example, thermal reradiation of the satellite is ignored, and vice versa. If a constrained value of 1 is employed, full confidence is placed in the SRP model.

In this study, we use the amplitude of circle-per-revolutions empirical accelerations to assess the magnitude of residual accelerations for LEO POD. The time series of the amplitude of the employed empirical acceleration and scaling parameters of the SRP are depicted in Figure 5. For the GRACE-FO satellites, the estimated empirical accelerations in the along-track and cross-track directions are mostly within  $30 \text{ nm/s}^2$ , and several fluctuations occur in 2019. The scale factors of the SRP vary between 0.5 and 1.5, and no significant correlation with  $\beta$ -angle is observed. For the HY-2B and Jason-3 satellites with altitudes of 970 and 1336 km, respectively, the acceleration due to SRP becomes more relevant. The empirical acceleration of the two altimetry satellites (HY-2B and Jason-3) in the along-track direction is within  $10 \text{ nm/s}^2$ , and the normal acceleration fluctuates frequently, especially for Jason-3 (fluctuations of around  $10 \text{ nm/s}^2$ ). For the Jason-3 satellite, there were 18 attitude maneuver events during 2019, and the continuous change of the satellite's attitude will inevitably affect the surface force, which may lead to some fluctuation in empirical acceleration. Scale parameters show a clear signature linked to the evolution of the  $\beta$ -angle for the two altimetry satellites. The introduction of TRP causes the apparent biases of the SRP scale for the different solutions in Figure 5. For solution NG1 (without TRP), the mean value of SRP scale factor is greater than 1, indicating that the SRP modeling is insufficient.

Figure 6 illustrates the variations in the empirical parameters due to the refinement of dynamic models, and the interquartile range (IQR, i.e.,  $Q_3 - Q_1$ ) is used for box-plots of the daily mean values of the empirical accelerations and SRP scale factors. The more accurate the modeling used to describe the solar radiation pressure of a LEO satellite, the closer the estimated scale parameter is to 1. The scale factor of solutions that ignore thermal reradiation (i.e., NG0, NG1, and NG2) ranges from 1.0 to 1.2, suggesting that the SRP modeling is insufficient. Although NG3 considers the instantaneous TRP, the scale parameters are in the range of 0.8–1.0, which clearly overestimates the TRP of the satellite. The SRP scaling parameter in solution NG4 exhibits a stable mean value, which is closer to 1. For the Jason-3 satellite with an independent solar panel, the improvement in the SRP scale is notable.

Variations in empirical accelerations occur mainly in the along-track direction for the GRACE-FO and HY-2B satellites with lower orbits. Tables S4 in Supporting Information S1 contains empirical parameters statistics of all assessed orbit solutions. Compared with the standard model (NG0 solution), the application of the enhanced dynamic model (NG4 solution) reduces the employed empirical acceleration in the along-track direction by 15% and 19% for GRACE-C and HY-2B, respectively (see Figure 7). The normal empirical acceleration caused by SRP modeling is slight, but it is significant in terms of the SRP scale factor. This trend is pronounced for the Jason-3 satellite. Mean empirical accelerations and reductions from different orbit solutions are displayed in Figure 7. The empirical acceleration reduction emphasizes the impact of each model extension. When the static temperature model (NG3) is applied to the Jason-3 spacecraft, an increase in the normal accelerations is visible. This phenomenon may result from mis-modeled thermal reradiation of the satellite, and it strongly depends on the shape of the solar panel. The effect is barely observed for the steady-state model (solution NG4).

For LEO satellites, the proportion of the penumbra period (e.g., the penumbra transition takes approximately 2 min when GRACE-C's  $\beta$  is approximately  $62^\circ$ ) is very small compared to the whole POD arc. From Tables S4 in Supporting Information S1 and Figure 7, the empirical parameters in solutions NG1 and NG2 are almost the same. Since only 1 year of data is used, the effect of time-dependent TSI products is very small but realistic, which

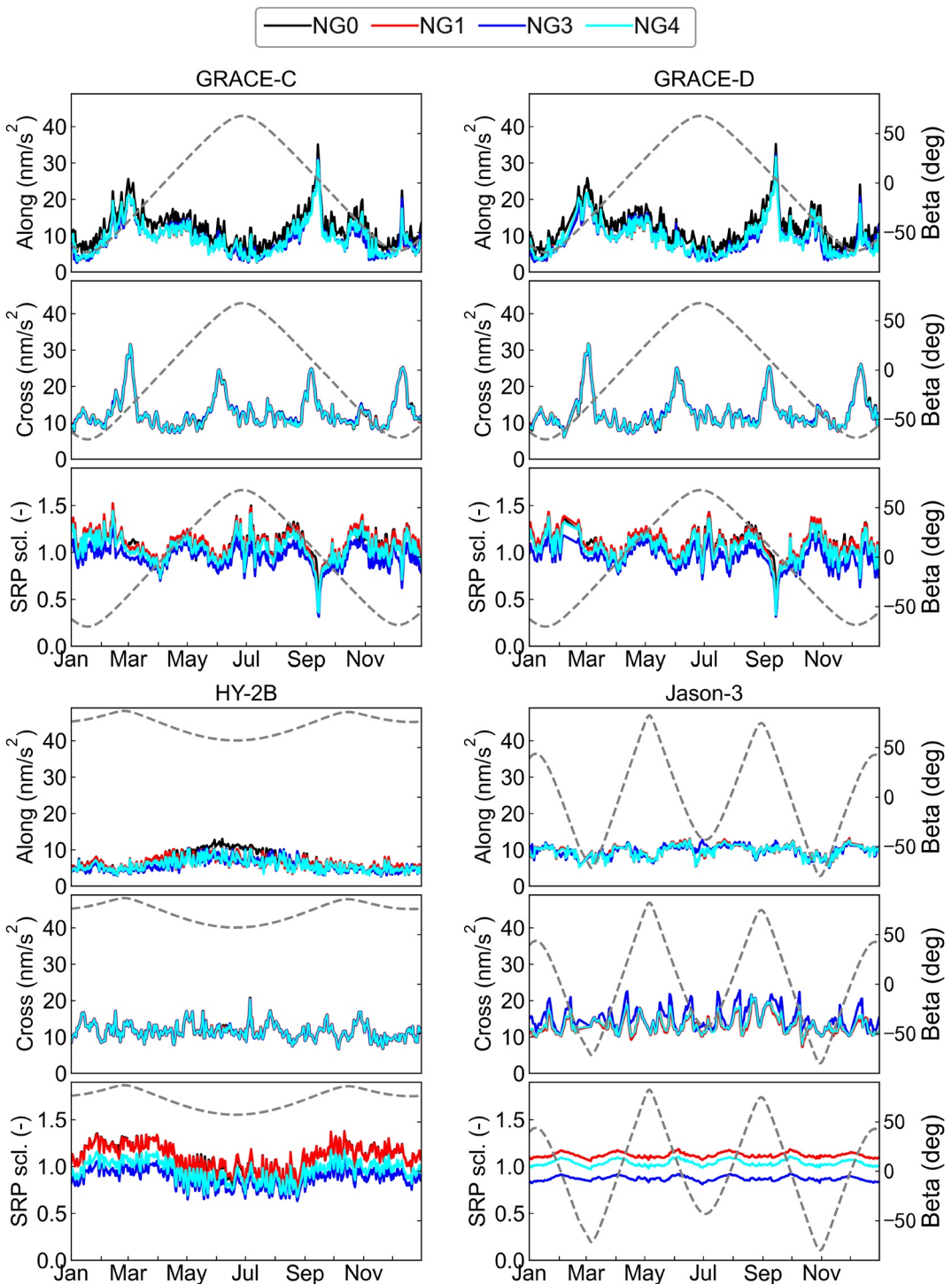


**Figure 5.** Daily mean values of the estimated empirical accelerations in the along-track and cross-track directions and scaling parameters of the SRP for the GRACE-FO, HY-2B, and Jason-3 satellites. The  $\beta$ -angle (the Sun's elevation above the orbital plane) is illustrated by a gray dotted line.

is in line with the flight environment of LEO satellites. It is important to note the improved correlation matrix of the final estimated orbital parameters (Figure 8). A strong correlation between the estimated scale parameter of the SRP and drag is noted for the NG0 solution, and reasonable results can be obtained when enhanced orbit modeling is applied (solution NG4). In addition, the correlation between the empirical acceleration and scale

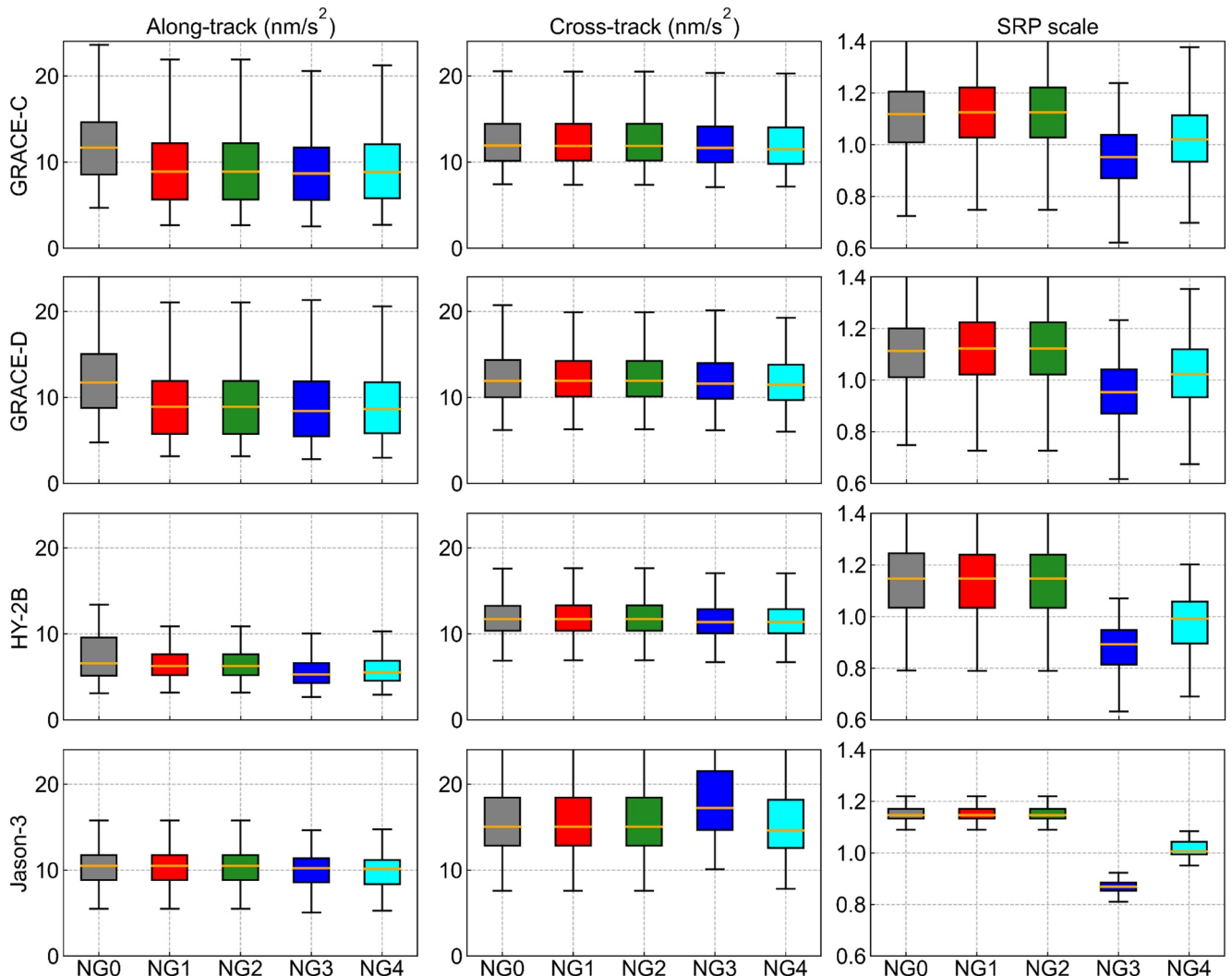


**Figure 6.** Estimated empirical accelerations decomposed into the along-track and cross-track directions and the SRP scale parameters for all orbit solutions. The box ranges from the first ( $Q_1$ ) to the third ( $Q_3$ ) quartile, and the horizontal orange line inside the box indicates the median. The top and bottom whiskers represent the maximum ( $Q_3 + 1.5 \cdot \text{IQR}$ ) and minimum ( $Q_1 - 1.5 \cdot \text{IQR}$ ), respectively.

factors is also improved for solution NG4. The correlation coefficients for solutions NG1 and NG3 are presented in Figure S2 of Supporting Information S1.

#### 4.2. Satellite Laser Ranging Validation

Satellite laser ranging is a powerful technique to validate the orbit accuracy of LEO satellites and is widely used by the LEO POD community for studies such as orbit evaluation, geodetic parameter estimation, and space ties between the GNSS and SLR (D. Arnold et al., 2018; M. R. Pearlman, Noll, et al., 2019; Y. C. Wang, Guo, et al., 2020)). In this paper, we focus on the contribution of SLR measurements to evaluate the orbit quality of different POD solutions. For SLR measurement preprocessing, it is necessary to consider the center-of-mass (CoM) correction of the laser retroreflector (LRR) trajectory and range correction, and reference values provided by (Grunwaldt, 2015) are used. In addition, the station-related corrections can significantly improve the SLR residuals, and implementation details are described in the Swarm and Sentinel-6A missions (D. Arnold et al., 2018; Montenbruck, Hackel, van den IJssel, & Arnold, 2018; Montenbruck, Hackel, et al., 2021). In this paper, 12 high-performance stations (Arequipa, Graz, Greenbelt, Haleakala, Hartebeesthoek, Herstmonceaux, Matera, Monument Peak, Mount Stromlo, Potsdam, Yarragadee, and Zimmerwald) of the ILRS network (M. R.

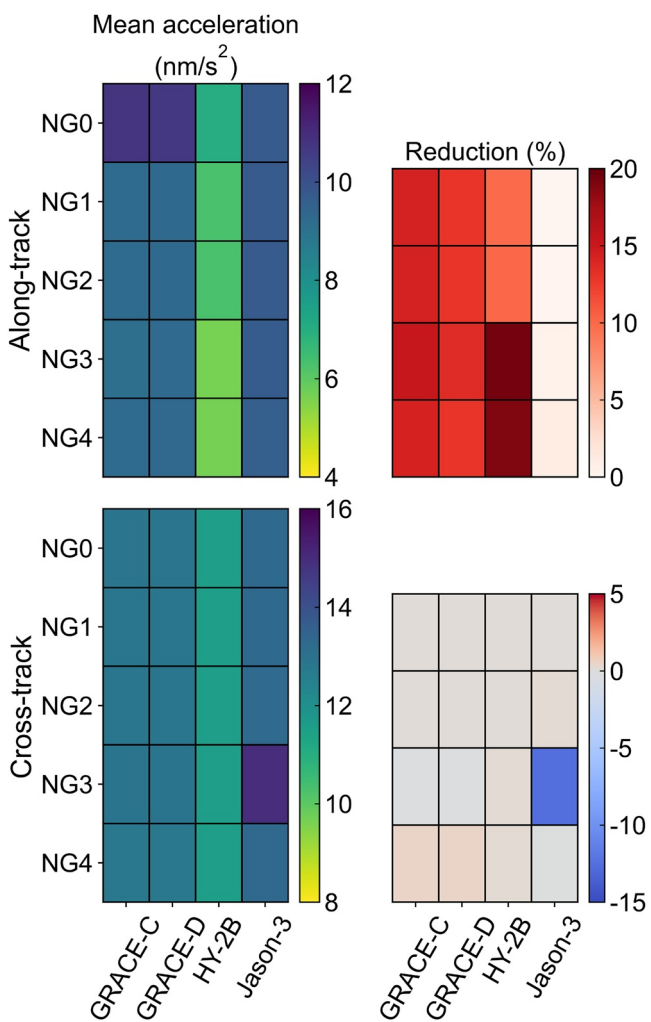


**Figure 7.** Average empirical acceleration (left column) and reduction w.r.t NG0 (right column) of different orbit solutions.

Pearlman, Noll, et al., 2019] with mm-to-cm-level precision are used, the data are considered for elevations above 8°, and a 15-cm threshold is used for data filtering.

For the GRACE-FO, HY-2B, and Jason-3 satellites, the SLR residuals of different POD solutions are shown in Figure 9. The improvement in SLR residuals is visible in solutions NG1, NG3, and NG4 for all LEO missions. For the simple static temperature model (NG3), the overestimated effect is noted in the empirical parameter statistics, but a reduction in the STD of the SLR residuals is obtained. This may result from the SRP scale factor absorbing the mis-modeled thermal reradiation. A negative offset of SLR residuals is found in solution NG3 for the GRACE-FO satellites. For the HY-2B and Jason-3 satellites, the improvement in the SLR residuals STD is approximately 0.5 mm for enhanced SRP modeling (solution NG4). The introduction of the enhanced SRP model diminished the mean offset of the SLR residuals by 1.2 and 0.7 mm for the HY-2B and Jason-3 satellites, respectively. A reduction of approximately 1 mm in the STD can be observed in the NG1 solution for the GRACE-FO satellites, and this improvement is driven by the new atmospheric density model for drag. The different elevations of the sun ( $\beta$ -angle) are shown in Figure 9. The sun-synchronous orbit (inclination 99.4°) is employed for HY-2B with a stable  $\beta$ -angle ranging between 57.3° and 86.7°.

For the Jason-3 satellite with a higher altitude, the orbit is more sensitive to the SRP model. The enhanced SRP modeling benefits the overall POD accuracy, and it also affects the estimation of the SRP scaling parameters. In other words, the refinement of the SRP modeling can put itself at a high confidence level to reduce excessive dependence on the scale parameter, which is closer to the real in-flight environment of the satellite. From Figure 9, there is no clear correlation between the SLR residuals and the  $\beta$ -angle for all satellites. Table 3 summarizes the mean and STD values of the SLR residuals for all solutions. A slight reduction in the STD of the SLR residuals is observed for the physical shadow model (solution NG2) when satellites are during eclipse periods.

For further analysis, SLR residuals as functions of the elongation angle are considered to evaluate two different TRP models of LEO satellites. Figure 10

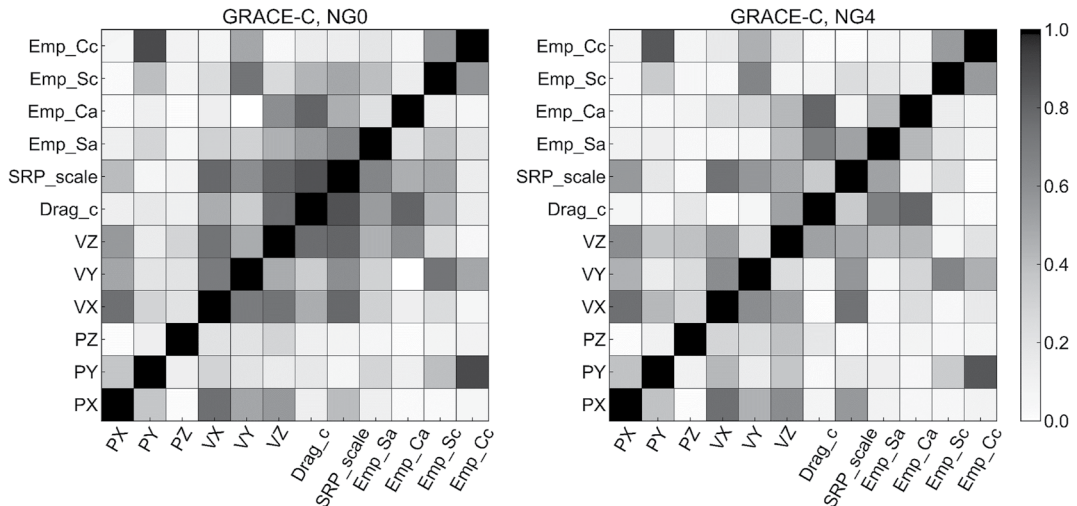


**Figure 8.** Correlation between the position (PX, PY, PZ) and velocity (VX, VY, VZ) at the initial epoch and the estimated parameters for the GRACE-FO satellite. The  $\beta$  angle is approximately 6°.

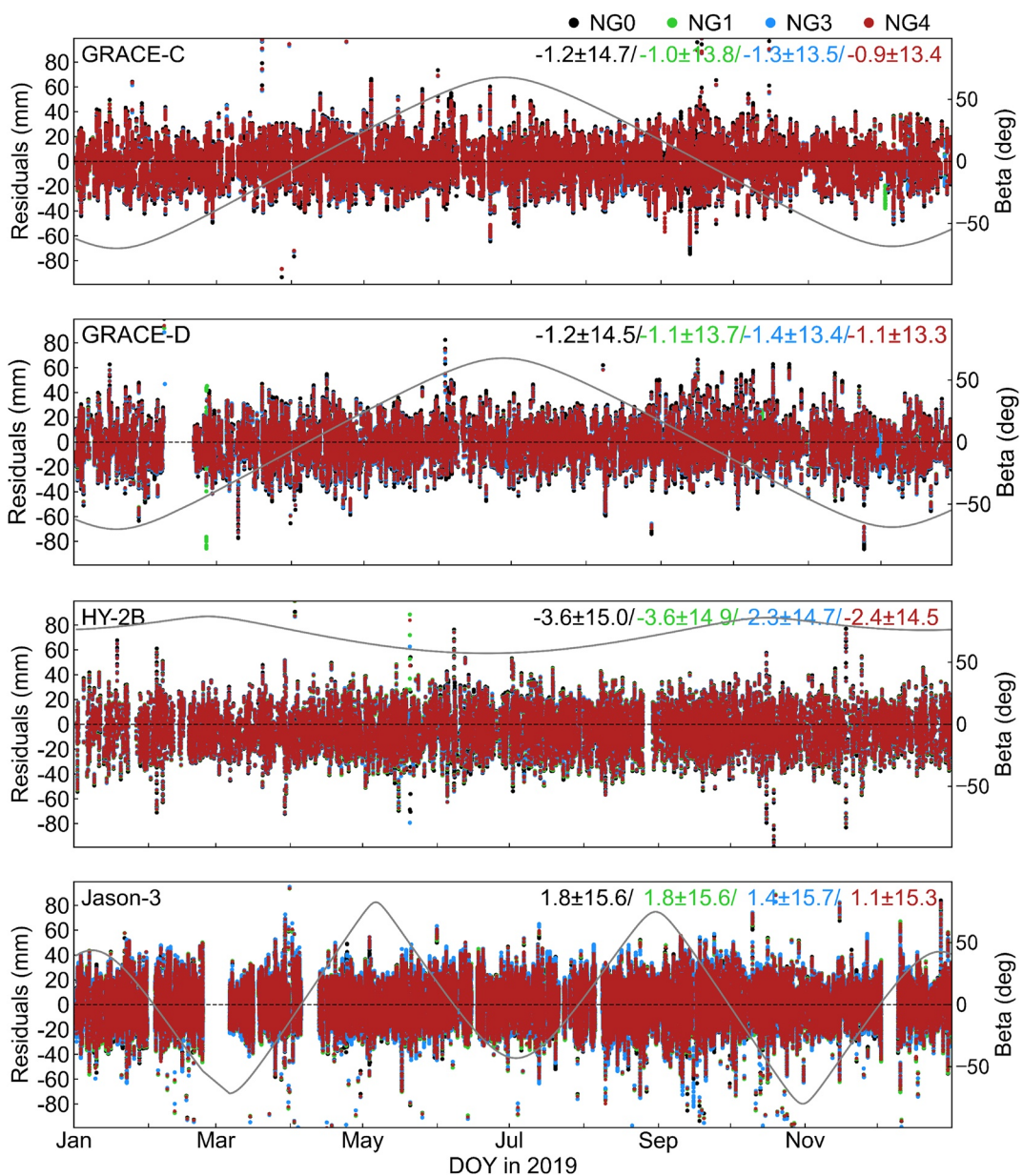


**Figure 9.** Satellite laser ranging residuals of the GRACE-FO, HY-2B, and Jason-3 satellites for the different orbit solutions in 2019. The  $\beta$ -angle is illustrated in gray. The mean and STD values of the SLR residuals are displayed in mm for each subplot.

**Table 3**

Mean and STD of the SLR Residuals for All Orbit Solutions (Unit: mm)

| Sol. ID | GRACE-C       |               | GRACE-D       |               | HY-2B         |               | Jason-3      |              |
|---------|---------------|---------------|---------------|---------------|---------------|---------------|--------------|--------------|
|         | All           | Eclipses      | All           | Eclipses      | All           | Eclipses      | All          | Eclipses     |
| NG0     | -1.2 +/- 14.7 | -0.4 +/- 13.9 | -1.2 +/- 14.5 | -0.2 +/- 13.9 | -3.6 +/- 15.0 | -3.1 +/- 14.7 | 1.8 +/- 15.6 | 0.8 +/- 15.1 |
| NG1     | -1.0 +/- 13.8 | -0.4 +/- 13.2 | -1.1 +/- 13.7 | -0.1 +/- 13.2 | -3.6 +/- 14.9 | -3.1 +/- 14.6 | 1.8 +/- 15.6 | 0.8 +/- 15.1 |
| NG2     | -0.9 +/- 13.8 | -0.4 +/- 13.1 | -1.1 +/- 13.6 | -0.1 +/- 13.1 | -3.6 +/- 14.9 | -3.1 +/- 14.5 | 1.8 +/- 15.6 | 0.8 +/- 15.0 |
| NG3     | -1.3 +/- 13.5 | -0.6 +/- 12.7 | -1.4 +/- 13.4 | -0.2 +/- 12.8 | -2.3 +/- 14.7 | -2.0 +/- 14.2 | 1.4 +/- 15.7 | 1.1 +/- 15.2 |
| NG4     | -0.9 +/- 13.4 | -0.5 +/- 12.6 | -1.1 +/- 13.3 | -0.1 +/- 12.7 | -2.4 +/- 14.5 | -1.9 +/- 14.1 | 1.1 +/- 15.3 | 0.6 +/- 14.7 |

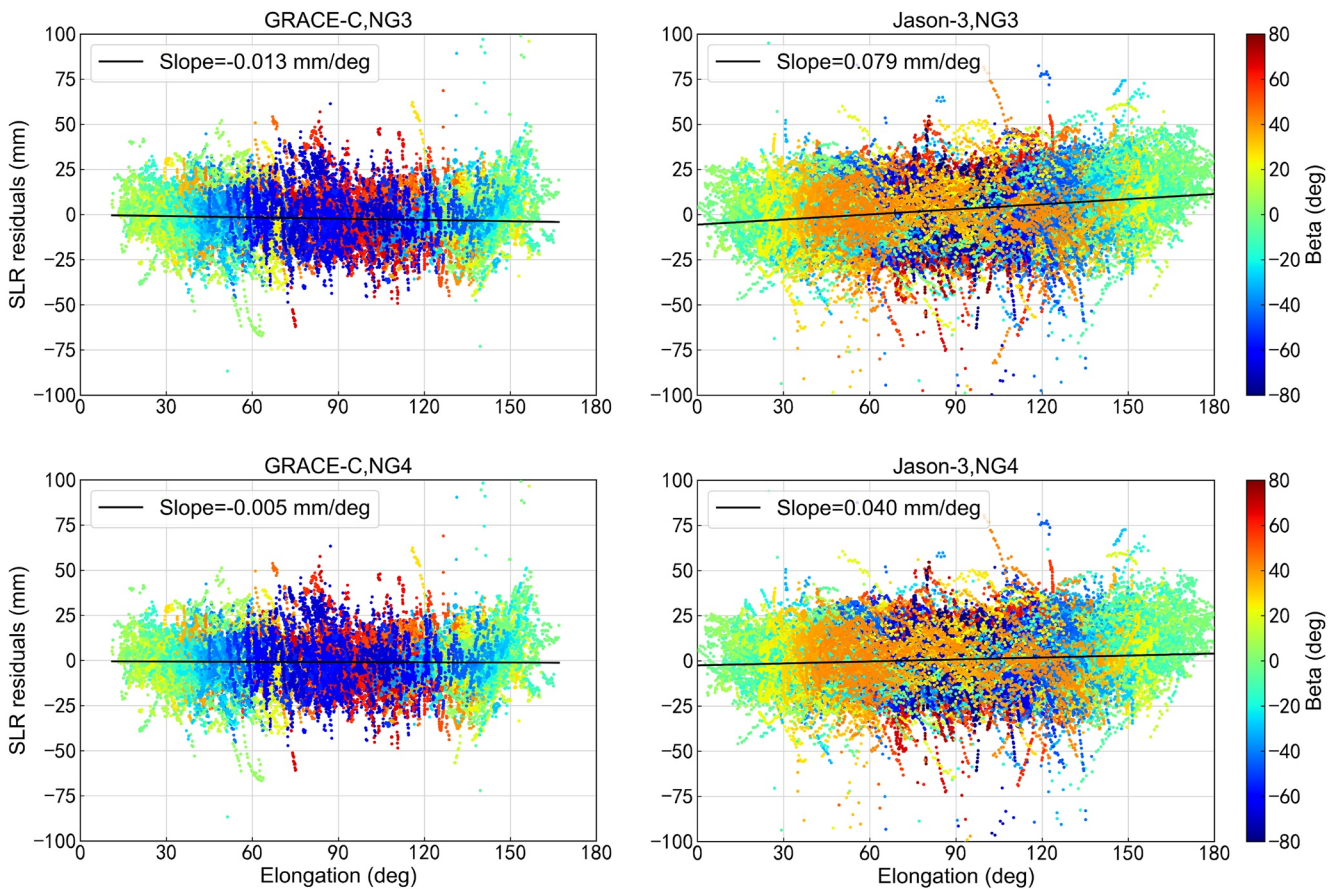


**Figure 10.** SLR residuals of the GRACE-C and Jason-3 satellites as a function of elongation of the Sun w.r.t the satellite for solutions NG3 (top) and NG4 (bottom). The fitted trend line is shown in black.

shows the linear dependency of the SLR residuals on the elongation angle (the angle between Earth and Sun as observed by a satellite). This potential trend (black line in Figure 10) revealed by SLR residuals may be related to insufficient modeling of SRP. For GRACE-C, the linear dependency between the SLR residuals and the elongation angle is  $-0.013 \text{ mm/deg}$  in the NG3 solution, while the correlation is close to zero for the NG4 solution with a 61% improvement. For the Jason-3 satellite, the linear correlation is reduced from  $0.079 \text{ mm/deg}$  to  $0.040 \text{ mm/deg}$  in the NG4 solution, resulting in a 49% improvement. In general, the advanced steady-state TRP model can significantly eliminate the SRP-related systematic errors revealed by the SLR observations, and the improved SRP can obtain a stable and reasonable estimation of the scaling parameter. The steady-state TRP model is more practical and improves the overall orbit quality of LEO satellites.

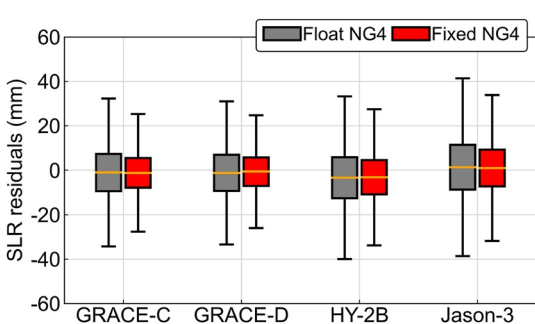


**Figure 11.** SLR residuals for the float and ambiguity-fixed orbit solution. The nomenclature of the box-whisker diagrams is consistent with Figure 6.

In addition, GNSS satellite biases provided by the CNES-CLS analysis center are employed to implement an ambiguity-fixed solution for LEO satellites based on solution NG4. The superior orbit quality of the ambiguity-fixed solution is visible when using the SLR technique as an independent validation tool (Figure 11). The implementation of ambiguity-fixed solutions can further improve the orbit accuracy based on enhanced non-gravitational force modeling, and the IQR of SLR residuals is reduced by 3–4 mm for all assessed satellites.

## 5. Conclusions

In this contribution, we focus on refined solar radiation pressure modeling acting on LEO satellites, and the potential approximation errors of existing

standard models are reduced by considering various physical effects. Time-dependent radiation data and physical shadow models are taken into account for the SRP. Two different TRP models are developed to address the absorbed SRP radiation of satellites. The latest DTM-2020 atmospheric density model is considered for drag calculations of the satellites. The data of the GRACE-FO, HY-2B, and Jason-3 satellites are used to assess the POD performance of the new strategies. Internal quality indexes (empirical orbit parameters) and external validation (independent SLR measurements) are considered to evaluate POD performance.

Based on the results of the empirical parameters, the refinement of the non-gravitational force modeling significantly reduces the dependence on empirical acceleration and the uncertainty in orbit determination. The magnitude of the estimated empirical acceleration using the enhanced POD solutions is reduced by approximately 19% and 15% for the GRACE-C and HY-2B satellites, respectively. The introduction of time-dependent solar flux and physical shadow functions has a slight effect on LEO POD. Considering the satellite geometry error, a dimensionless scaling parameter for the SRP is used to address prevailing uncertainties in the orbit determinations. Stable scaling parameters are obtained when a more realistic steady-state temperature model is considered for the TRP of the satellite, which can significantly reduce the overestimated effect due to the simple static temperature model.

The SLR provides a powerful means to validate the POD performance of the improved dynamics model. With the enhanced non-gravitational force models, the SLR validation shows the best orbit solutions with RMS values of 10.4, 10.1, 12.4, and 13.2 mm for the GRACE-C, GRACE-D, HY-2B, and Jason-3 satellites, respectively. The enhanced TRP model reduces the remaining systematic errors in the analytical SRP models. For the GRACE-C and Jason-3 satellites, the linear dependency of the SLR residuals on the elongation is reduced notably with improvements of approximately 61% and 46%, respectively.

In summary, enhanced non-gravitational force modeling results in reduced dependence on empirical parameters, elimination of potential systematic biases, and improvement in the overall orbit quality of LEO satellites. This is verified from the orbit determination results of four satellites, which is also in accord with the space geodesy community's goal to pursue the best-possible orbit solution. The enhanced models used in this paper are applicable to other LEO missions and the calibration of accelerometers. The non-gravitational forces are established on the basis of a satellite macro-model, and the panel material properties involved in the radiation pressure model directly affect the calculation of the SRP acceleration. These parameters are usually provided by the spacecraft manufacturer with a nominal prior accuracy. At the end of a mission, the aging of satellite surface materials will inevitably introduce systematic errors to the SRP or drag.

Future work can focus on satellite geometry modeling. More advanced macro models, such as finite elements, may be considered to improve the accuracy of acceleration calculations from non-gravitational force. For radiation models, providing satellite surface radiation coefficients across the full wavelength band is expected to be in line with the real in-flight environment. The development of an adjusted analytical SRP pressure can address the variations in satellite surface parameters. In addition, the refinement of conservative force models and external auxiliary data employed in POD should be considered, such as the introduction of high-precision time-varying gravity fields and tide model updates, as well as time-varying surface radiation datasets. For GNSS satellites, analytical models may not be used due to a lack of prior information, as empirical models are employed. With the availability of GNSS satellite material properties, the analytical model is more realistic, which is useful for both high-precision POD and orbit prediction.

## Data Availability Statement

The GRACE-FO Level-1B data used in this study have kindly been accessed from German GeoforschungsZentrum (GFZ) Information System and Data Center at <https://isdc.gfz-potsdam.de/homepage/>. The onboard data of Jason-3 satellites can be obtained from <https://www.aviso.altimetry.fr/en/data/data-access/ftp.html>. HY-2B flight data are provided by the National Satellite Ocean Application Service of China (NSOAS). The CERES SYN1deg data can be obtained from the NASA Langley Research Center CERES ordering tool at <https://ceres.larc.nasa.gov/>. The GNSS precise orbit and clock product are publicly available at <https://cddis.nasa.gov/archive/gnss/products>. The SLR observations of LEO satellites are provided by ILRS at [https://cddis.nasa.gov/archive/slrf/data/npt\\_crd](https://cddis.nasa.gov/archive/slrf/data/npt_crd).

## Acknowledgments

This study was supported by the National Natural Science Foundation of China (Grants 42074032, 41931075, 42030109, 42204020, and 4204020). We are grateful to International GNSS Service (IGS) and the International Satellite Laser Ranging Service (ILRS) for providing publicly available GNSS and SLR data. We also appreciate two anonymous reviewers and the responsible editor for their valuable comments and improvements to this manuscript.

## References

- Abich, K., Abramovici, A., Amparan, B., Baatzsch, A., Okihiro, B. B., Barr, D. C., et al. (2019). In-orbit performance of the GRACE Follow-on laser ranging interferometer. *Physical Review Letters*, 123(3), 031101. <https://doi.org/10.1103/PhysRevLett.123.031101>
- Adhya, S. (2005). *Thermal re-radiation modelling for the precise prediction and determination of spacecraft orbits*. University College London.
- Appleby, G., Rodríguez, J., & Altamimi, Z. (2016). Assessment of the accuracy of global geodetic satellite laser ranging observations and estimated impact on ITRF scale: Estimation of systematic errors in LAGEOS observations 1993–2014. *Journal of Geodesy*, 90(12), 1371–1388. <https://doi.org/10.1007/s00190-016-0929-2>
- Arnold, D., Meindl, M., Beutler, G., Dach, R., Schaer, S., Lutz, S., et al. (2015). CODE's new solar radiation pressure model for GNSS orbit determination. *Journal of Geodesy*, 89(8), 775–791. <https://doi.org/10.1007/s00190-015-0814-4>
- Arnold, D., Montenbruck, O., Hackel, S., & Sośnica, K. (2018). Satellite laser ranging to low Earth orbiters: Orbit and network validation. *Journal of Geodesy*, 93(11), 2315–2334. <https://doi.org/10.1007/s00190-018-1140-4>
- Banville, S., Geng, J., Loyer, S., Schaer, S., Springer, T., & Strasser, S. (2020). On the interoperability of IGS products for precise point positioning with ambiguity resolution. *Journal of Geodesy*, 94(1), 10. <https://doi.org/10.1007/s00190-019-01335-w>
- Bertiger, W., Desai, S. D., Haines, B., Harvey, N., Moore, A. W., Owen, S., & Weiss, J. P. (2010). Single receiver phase ambiguity resolution with GPS data. *Journal of Geodesy*, 84(5), 327–337. <https://doi.org/10.1007/s00190-010-0371-9>
- Bertiger, W. I., Bar-Sever, Y. E., Christensen, E. J., Davis, E. S., Guinn, J. R., Haines, B. J., et al. (1994). GPS precise tracking of TOPEX/POSEIDON: Results and implications. *Journal of Geophysical Research*, 99(C12), 24449. <https://doi.org/10.1029/94jc01171>
- Bock, H., Jäggi, A., Beutler, G., & Meyer, U. (2014). GOCE: Precise orbit determination for the entire mission. *Journal of Geodesy*, 88(11), 1047–1060. <https://doi.org/10.1007/s00190-014-0742-8>
- Bruinsma, S., & Bonifacé, C. (2021). The operational and research DTM-2020 thermosphere models. *Journal of Space Weather and Space Climate*, 11, 47. <https://doi.org/10.1051/swsc/2021032>
- Bury, G., Sośnica, K., Zajdel, R., & Strugarek, D. (2020). Toward the 1-cm Galileo orbits: Challenges in modeling of perturbing forces. *Journal of Geodesy*, 94(2), 16. <https://doi.org/10.1007/s00190-020-01342-2>
- CERES, S. T. (2017). In C. S. Team (Ed.), *CERES and GEO-enhanced TOA, within-atmosphere and surface fluxes, clouds and aerosols 1-hourly terra-aqua edition4A*.
- Cerri, L., Berthias, J. P., Bertiger, W. I., Haines, B. J., Lemoine, F. G., Mercier, F., et al. (2010). Precision orbit determination standards for the Jason series of altimeter missions. *Marine Geodesy*, 33(1), 379–418. <https://doi.org/10.1080/01490419.2010.488966>
- Dewitte, S., & Nevens, S. (2016). The total solar irradiance climate data record. *The Astrophysical Journal*, 830(1), 25. <https://doi.org/10.3847/0004-637x/830/1/25>
- Doornbos, E. (2012). *Thermospheric density and wind determination from satellite dynamics*. Springer Science & Business Media. <https://doi.org/10.1007/978-3-642-25129-0>
- Dow, J. M., Neilan, R. E., & Rizos, C. (2009). The international GNSS Service in a changing landscape of global navigation satellite systems. *Journal of Geodesy*, 83(3–4), 191–198. <https://doi.org/10.1007/s00190-008-0300-3>
- Duan, B., Hugentobler, U., Hofacker, M., & Selmke, I. (2020). Improving solar radiation pressure modeling for GLONASS satellites. *Journal of Geodesy*, 94(8), 72. <https://doi.org/10.1007/s00190-020-01400-9>
- Fernández, M., Peter, H., Arnold, D., Duan, B., Simons, W., Wermuth, M., et al. (2022). Copernicus Sentinel-1 POD reprocessing campaign. *Advances in Space Research*, 70(2), 249–267. <https://doi.org/10.1016/j.asr.2022.04.036>
- Flohrer, C., Otten, M., Springer, T., & Dow, J. (2011). Generating precise and homogeneous orbits for Jason-1 and Jason-2. *Advances in Space Research*, 48(1), 152–172. <https://doi.org/10.1016/j.asr.2011.02.017>
- Friis-Christensen, E., Lühr, H., Knudsen, D., & Haagmans, R. (2008). Swarm—An Earth observation mission investigating geospace. *Advances in Space Research*, 41(1), 210–216. <https://doi.org/10.1016/j.asr.2006.10.008>
- Fröhlich, C., & Lean, J. (2004). Solar radiative output and its variability: Evidence and mechanisms. *Astronomy and Astrophysics Review*, 12(4), 273–320. <https://doi.org/10.1007/s00159-004-0024-1>
- Geng, J., Chen, X., Pan, Y., & Zhao, Q. (2019). A modified phase clock/bias model to improve PPP ambiguity resolution at Wuhan University. *Journal of Geodesy*, 93(10), 2053–2067. <https://doi.org/10.1007/s00190-019-01301-6>
- Grunwaldt, L. (2015). GRACE follow-on laser retro reflector user manual. Retrieved from [https://ilrs.gsfc.nasa.gov/docs/2015/GFO-MA-GFZ-LR-0001\\_2.pdf](https://ilrs.gsfc.nasa.gov/docs/2015/GFO-MA-GFZ-LR-0001_2.pdf)
- Hackel, S., Montenbruck, O., Steigenberger, P., Balss, U., Gisinger, C., & Eineder, M. (2016). Model improvements and validation of TerraSAR-X precise orbit determination. *Journal of Geodesy*, 91(5), 547–562. <https://doi.org/10.1007/s00190-016-0982-x>
- Haines, B., Bar-Sever, Y., Bertiger, W., Desai, S., & Willis, P. (2004). One-centimeter orbit determination for Jason-1: New GPS-based strategies. *Marine Geodesy*, 27(1–2), 299–318. <https://doi.org/10.1080/01490410490465300>
- ILRS. (2020). SLRF2014 station coordinates. Retrieved from [ftp://gdc.cddis.eosdis.nasa.gov/pub/slrf/products/resource/SLRF2014\\_POS+VEL\\_2030.0\\_200325.snx](ftp://gdc.cddis.eosdis.nasa.gov/pub/slrf/products/resource/SLRF2014_POS+VEL_2030.0_200325.snx)
- Jäggi, A., Dach, R., Montenbruck, O., Hugentobler, U., Bock, H., & Beutler, G. (2009). Phase center modeling for LEO GPS receiver antennas and its impact on precise orbit determination. *Journal of Geodesy*, 83(12), 1145–1162. <https://doi.org/10.1007/s00190-009-0333-2>
- Jäggi, A., Dahle, C., Arnold, D., Bock, H., Meyer, U., Beutler, G., & van den IJssel, J. (2016). Swarm kinematic orbits and gravity fields from 18 months of GPS data. *Advances in Space Research*, 57(1), 218–233. <https://doi.org/10.1016/j.asr.2015.10.035>
- Kang, Z., Bettadpur, S., Nagel, P., Save, H., Poole, S., & Pie, N. (2020). GRACE-FO precise orbit determination and gravity recovery. *Journal of Geodesy*, 94(9), 85. <https://doi.org/10.1007/s00190-020-01414-3>
- Kang, Z., Tapley, B., Bettadpur, S., Ries, J., Nagel, P., & Pastor, R. (2006). Precise orbit determination for the GRACE mission using only GPS data. *Journal of Geodesy*, 80(6), 322–331. <https://doi.org/10.1007/s00190-006-0073-5>
- Knoche, P., Ries, J., & Tapley, B. (1988). Earth radiation pressure effects on satellites. In *Astrodynamics conference*. <https://doi.org/10.2514/6.1988-4292>
- Kopp, G., & Lean, J. L. (2011). A new, lower value of total solar irradiance: Evidence and climate significance. *Geophysical Research Letters*, 38(1), L01706. <https://doi.org/10.1029/2010gl045777>
- Kornfeld, R. P., Arnold, B. W., Gross, M. A., Dahya, N. T., Klipstein, W. M., Gath, P. F., & Bettadpur, S. (2019). GRACE-FO: The gravity recovery and climate experiment follow-on mission. *Journal of Spacecraft and Rockets*, 56(3), 931–951. <https://doi.org/10.2514/1.A34326>
- Lambin, J., Morrow, R., Fu, L.-L., Willis, J. K., Bonekamp, H., Lillibridge, J., et al. (2010). The OSTM/Jason-2 mission. *Marine Geodesy*, 33(S1), 4–25. <https://doi.org/10.1080/01490419.2010.491030>

- Landerer, F. W., Flechtner, F. M., Save, H., Webb, F. H., Bandikova, T., Bertiger, W. I., et al. (2020). Extending the global mass change data record: GRACE follow-on instrument and science data performance. *Geophysical Research Letters*, 47(12), e2020GL088306. <https://doi.org/10.1029/2020gl088306>
- Li, M., Li, W. W., Shi, C., Jiang, K. C., Guo, X., Dai, X. L., et al. (2017). Precise orbit determination of the Fengyun-3C satellite using onboard GPS and BDS observations. *Journal of Geodesy*, 91(11), 1313–1327. <https://doi.org/10.1007/s00190-017-1027-9>
- Lin, M., & Jia, Y. (2022). Past, present and future marine microwave satellite missions in China. *Remote Sensing*, 14(6), 1330. <https://doi.org/10.3390/rs14061330>
- Liu, J., & Ge, M. (2003). PANDA software and its preliminary result of positioning and orbit determination. *Wuhan University Journal of Natural Sciences*, 8(2), 603–609. <https://doi.org/10.1007/bf02899825>
- Loyer, S., Perosanz, F., Mercier, F., Capdeville, H., & Marty, J.-C. (2012). Zero-difference GPS ambiguity resolution at CNES-CLS IGS analysis center. *Journal of Geodesy*, 86(11), 991–1003. <https://doi.org/10.1007/s00190-012-0559-2>
- Lyard, F., Lefevre, F., Letellier, T., & Francis, O. (2006). Modelling the global ocean tides: Modern insights from FES2004. *Ocean Dynamics*, 56(5), 394–415. <https://doi.org/10.1007/s10236-006-0086-x>
- Mao, X., Arnold, D., Girardin, V., Villiger, A., & Jäggi, A. (2021). Dynamic GPS-based LEO orbit determination with 1 cm precision using the Bernese GNSS Software. *Advances in Space Research*, 67(2), 788–805. <https://doi.org/10.1016/j.asr.2020.10.012>
- March, G., Doornbos, E. N., & Visser, P. N. A. M. (2019). High-fidelity geometry models for improving the consistency of CHAMP, GRACE, GOCE and Swarm thermospheric density data sets. *Advances in Space Research*, 63(1), 213–238. <https://doi.org/10.1016/j.asr.2018.07.009>
- Marshall, J. A., & Luthcke, S. B. (1994). Modeling radiation forces acting on Topex/Poseidon for precision orbit determination. *Journal of Spacecraft and Rockets*, 31(1), 99–105. <https://doi.org/10.2514/3.26408>
- Mendes, V. B., & Pavlis, E. C. (2004). High-accuracy zenith delay prediction at optical wavelengths. *Geophysical Research Letters*, 31(14), L14602. <https://doi.org/10.1029/2004gl020308>
- Milani, A., Nobili, A. M., & Farinella, P. (1987). Non-gravitational perturbations and satellite geodesy.
- Montenbruck, O., Gill, E., & Lutz, F. H. (2002). Satellite orbits: Models, methods, and applications. *Applied Mechanics Reviews*, 55(2), B27–B28. <https://doi.org/10.1115/1.1451162>
- Montenbruck, O., Hackel, S., & Jäggi, A. (2018). Precise orbit determination of the Sentinel-3A altimetry satellite using ambiguity-fixed GPS carrier phase observations. *Journal of Geodesy*, 92(7), 711–726. <https://doi.org/10.1007/s00190-017-1090-2>
- Montenbruck, O., Hackel, S., van den IJssel, J., & Arnold, D. (2018). Reduced dynamic and kinematic precise orbit determination for the Swarm mission from 4 years of GPS tracking. *GPS Solutions*, 22(3), 79. <https://doi.org/10.1007/s10291-018-0746-6>
- Montenbruck, O., Hackel, S., Wermuth, M., & Zangerl, F. (2021). Sentinel-6A precise orbit determination using a combined GPS/Galileo receiver. *Journal of Geodesy*, 95(9), 109. <https://doi.org/10.1007/s00190-021-01563-z>
- Montenbruck, O., Kunzi, F., & Hauschild, A. (2021). Performance assessment of GNSS-based real-time navigation for the Sentinel-6 spacecraft. *GPS Solutions*, 26(1), 12. <https://doi.org/10.1007/s10291-021-01198-9>
- Montenbruck, O., Steigenberger, P., & Hugentobler, U. (2014). Enhanced solar radiation pressure modeling for Galileo satellites. *Journal of Geodesy*, 89(3), 283–297. <https://doi.org/10.1007/s00190-014-0774-0>
- Nasa/Larc/Sd/Asdc. (2019). In Team, C. S. (Ed.), *CERES energy balanced and filled (EBAF) TOA monthly means data in netCDF Edition4.1*. NSOAS. (2021). HY-2: A marine remote sensing satellite series planned by China. *National Satellite Ocean Application Service*. Retrieved from <http://www.nsoas.org.cn/index.html>
- Park, R. S., Folkner, W. M., Williams, J. G., & Boggs, D. H. (2021). The JPL planetary and lunar ephemerides DE440 and DE441. *The Astronomical Journal*, 161(3), 105. <https://doi.org/10.3847/1538-3881/abd414>
- Pearlman, M., Arnold, D., Davis, M., Barlier, F., Biancale, R., Vasilić, V., et al. (2019). Laser geodetic satellites: A high-accuracy scientific tool. *Journal of Geodesy*, 93(11), 2181–2194. <https://doi.org/10.1007/s00190-019-01228-y>
- Pearlman, M. R., Noll, C. E., Pavlis, E. C., Lemoine, F. G., Combrink, L., Degnan, J. J., et al. (2019). The ILRS: Approaching 20 years and planning for the future. *Journal of Geodesy*, 93(11), 1–20. <https://doi.org/10.1007/s00190-019-01241-1>
- Pérez, D., & Bevilacqua, R. (2015). Neural network based calibration of atmospheric density models. *Acta Astronautica*, 110, 58–76. <https://doi.org/10.1016/j.actaastro.2014.12.018>
- Petit, G., & Luzum, B. (2010). IERS conventions (2010)Rep. Bureau International des Poids et mesures sevres (France).
- Prölls, G. W., & Bird, M. K. (2004). Physics of the Earth's space environment: An introduction.
- Robertson, R., Flury, J., Bandikova, T., & Schilling, M. (2015). Highly physical penumbra solar radiation pressure modeling with atmospheric effects. *Celestial Mechanics and Dynamical Astronomy*, 123(2), 169–202. <https://doi.org/10.1007/s10569-015-9637-0>
- Robertson, R. V. (2015). Highly physical solar radiation pressure modeling during penumbra transitions.
- Rodriguez-Solano, C. J., Hugentobler, U., Steigenberger, P., & Lutz, S. (2011). Impact of Earth radiation pressure on GPS position estimates. *Journal of Geodesy*, 86(5), 309–317. <https://doi.org/10.1007/s00190-011-0517-4>
- Schaer, S., Villiger, A., Arnold, D., Dach, R., Prange, L., & Jäggi, A. (2021). The CODE ambiguity-fixed clock and phase bias analysis products: Generation, properties, and performance. *Journal of Geodesy*, 95(7), 81. <https://doi.org/10.1007/s00190-021-01521-9>
- Schmid, R., Dach, R., Collilieux, X., Jäggi, A., Schmitz, M., & Dilssner, F. (2016). Absolute IGS antenna phase center model igs08.atx: Status and potential improvements. *Journal of Geodesy*, 90(4), 343–364. <https://doi.org/10.1007/s00190-015-0876-3>
- Shako, R., Förste, C., Abrilovskov, O., Bruinsma, S., Marty, J.-C., Lemoine, J.-M., et al. (2014). EIGEN-6C: A high-resolution global gravity combination model including GOCE data. In F. Flechtner, N. Sneeuw, & W.-D. Schuh (Eds.), *Observation of the system Earth from space—CHAMP, GRACE, GOCE and future missions* (pp. 155–161). Springer Berlin Heidelberg. [https://doi.org/10.1007/978-3-642-32135-1\\_20](https://doi.org/10.1007/978-3-642-32135-1_20)
- Standish, E. M., & Williams, J. G. (1992). Orbital ephemerides of the Sun, Moon, and planets. In *Explanatory supplement to the astronomical almanac* (pp. 279–323).
- Tapley, B. D., Bettadpur, S., Ries, J. C., Thompson, P. F., & Watkins, M. M. (2004). GRACE measurements of mass variability in the Earth system. *Science*, 305(5683), 503–505. <https://doi.org/10.1126/science.1099192>
- Vallado, D. A., & Finkelman, D. (2014). A critical assessment of satellite drag and atmospheric density modeling. *Acta Astronautica*, 95, 141–165. <https://doi.org/10.1016/j.actaastro.2013.10.005>
- van den IJssel, J., Encarnaçao, J., Doornbos, E., & Visser, P. (2015). Precise science orbits for the Swarm satellite constellation. *Advances in Space Research*, 56(6), 1042–1055. <https://doi.org/10.1016/j.asr.2015.06.002>
- Vielberg, K., & Kusche, J. (2020). Extended forward and inverse modeling of radiation pressure accelerations for LEO satellites. *Journal of Geodesy*, 94(4), 43. <https://doi.org/10.1007/s00190-020-01368-6>
- Visser, T., March, G., Doornbos, E., de Visser, C., & Visser, P. (2019). Horizontal and vertical thermospheric cross-wind from GOCE linear and angular accelerations. *Advances in Space Research*, 63(10), 3139–3153. <https://doi.org/10.1016/j.asr.2019.01.030>

- Wang, J., Aouf, L., Jia, Y., & Zhang, Y. (2020). Validation and calibration of significant wave height and wind speed retrievals from HY2B altimeter based on deep learning. *Remote Sensing*, 12(17), 2858. <https://doi.org/10.3390/rs12172858>
- Wang, Y. C., Guo, J. Y., Zhou, M. S., Jin, X., Zhao, C. M., & Chang, X. T. (2020). Geometric solution method of SLR station coordinate based on multi-LEO satellites. *Chinese Journal of Geophysics*, 63(12), 4333–4344. <https://doi.org/10.6038/cjg202000069>
- Wang, Y. C., Li, M., Jiang, K. C., Li, W. W., Qin, G., Zhao, Q. L., et al. (2021). Reduced-dynamic precise orbit determination of Haiyang-2B altimetry satellite using a refined empirical acceleration model. *Remote Sensing*, 13(18), 3702. <https://doi.org/10.3390/rs13183702>
- Woske, F., Kato, T., Rievers, B., & List, M. (2019). GRACE accelerometer calibration by high precision non-gravitational force modeling. *Advances in Space Research*, 63(3), 1318–1335. <https://doi.org/10.1016/j.asr.2018.10.025>
- Wu, S. C., Yunck, T. P., & Thornton, C. L. (1991). Reduced-dynamic technique for precise orbit determination of low Earth satellites. *Journal of Guidance, Control, and Dynamics*, 14(1), 24–30. <https://doi.org/10.2514/3.20600>
- Zajdel, R., Kazmierski, K., & Sośnica, K. (2022). Orbital artifacts in Multi-GNSS precise point positioning time series. *Journal of Geophysical Research: Solid Earth*, 127(2), e2021JB022994. <https://doi.org/10.1029/2021jb022994>
- Zhang, K., Li, X., Wu, J., Yuan, Y., Li, X., Zhang, X., & Zhang, W. (2021). Precise orbit determination for LEO satellites with ambiguity resolution: Improvement and comparison. *Journal of Geophysical Research: Solid Earth*, 126(9), e2021JB022491. <https://doi.org/10.1029/2021jb022491>
- Zhao, Q., Guo, J., Wang, C., Lyu, Y., Xu, X., Yang, C., & Li, J. (2022). Precise orbit determination for BDS satellites. *Satellite Navigation*, 3(1), 2. <https://doi.org/10.1186/s43020-021-00062-y>